NANO LETTERS

pubs.acs.org/NanoLett

Letter

Enhanced High Thermal Conductivity Cellulose Filaments via Hydrodynamic Focusing

Guantong Wang, Masaki Kudo, Kazuho Daicho, Sivasankaran Harish, Bin Xu, Cheng Shao, Yaerim Lee, Yuxuan Liao, Naoto Matsushima, Takashi Kodama, Fredrik Lundell, L. Daniel Söderberg, Tsuguyuki Saito, and Junichiro Shiomi*

Cite This: *Nano Lett.* 2022, 22, 8406−8412

Read Online

ACCESS | Metrics & More | Article Recommendations | Supporting Information

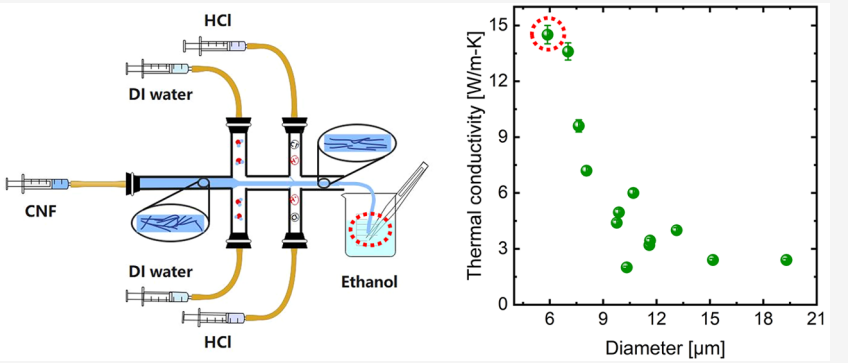

ABSTRACT: Nanocellulose is regarded as a green and renewable nanomaterial that has attracted increased attention. In this study, we demonstrate that nanocellulose materials can exhibit high thermal conductivity when their nanofibrils are highly aligned and bonded in the form of filaments. The thermal conductivity of individual filaments, consisting of highly aligned cellulose nanofibrils, fabricated by the flow-focusing method is measured in dried condition using a T-type measurement technique. The maximum thermal conductivity of the nanocellulose filaments obtained is 14.5 W/m-K, which is approximately five times higher than those of cellulose nanopaper and cellulose nanocrystals. Structural investigations suggest that the crystallinity of the filament remarkably influence their thermal conductivity. Smaller diameter filaments with higher crystallinity, that is, more internanofibril hydrogen bonds and less intrananofibril disorder, tend to have higher thermal conductivity. Temperature-dependence measurements also reveal that the filaments exhibit phonon transport at effective dimension between 2D and 3D.

KEYWORDS: *Nanocellulose, filament, flow focusing, thermal conductivity, crystallinity*

Nanocellulose is considered a renewable resource that can be obtained from many types of plant resources, such as wood, tunicates, and bacteria.[1] In addition to environmental friendliness, it possesses many advantages, such as outstanding mechanical properties,[2] lightweight (~1.6 g/cm^3), and high strength (~3 GPa), stiffness (~130 GPa), and flexibility.[3] Given these excellent properties, nanocellulose is used in wall and roof cavities in building systems to insulate heat, reduce noise, and provide draft protection. It is also used in ink dispersants for ballpoint pens,[3] disposable diapers with deodorizing functions for health-care assistants,[3] and aerogels with high strength (10 MPa) and Young's modulus (290 MPa), moderate light permeability, and good thermal insulation (0.06−0.07 W/m-K) properties.[4] Many studies on cellulose aerogels with low thermal conductivity have been reported. For example, Danny et al. prepared cellulose-based aerogels for use as thermal insulation in buildings and obtained a low thermal conductivity of <0.025 W/m-K.[5] Sakai et al. synthesized freeze-dried aerogels with even lower thermal conductivity (0.018−0.021 W/m-K).[6,7]

Cellulose materials for thermal insulation have been widely investigated, but only a limited number of studies on cellulose materials with enhanced heat conduction are available. Uetani et al. developed a flexible polymeric material by simply drawing cellulose hydrogels and found that the highest in-plane thermal conductivity of the cellulose nanopapers could reach 2.5 W/m-K.[8] Nanocellulose materials exhibit features that could render them viable high thermal conductors because cellulose molecules form polymer chains, and numerous studies on

Received: May 23, 2022
Revised: October 2, 2022
Published: October 25, 2022

https://doi.org/10.1021/acs.nanolett.2c02057
Nano Lett. 2022, 22, 8406−8412

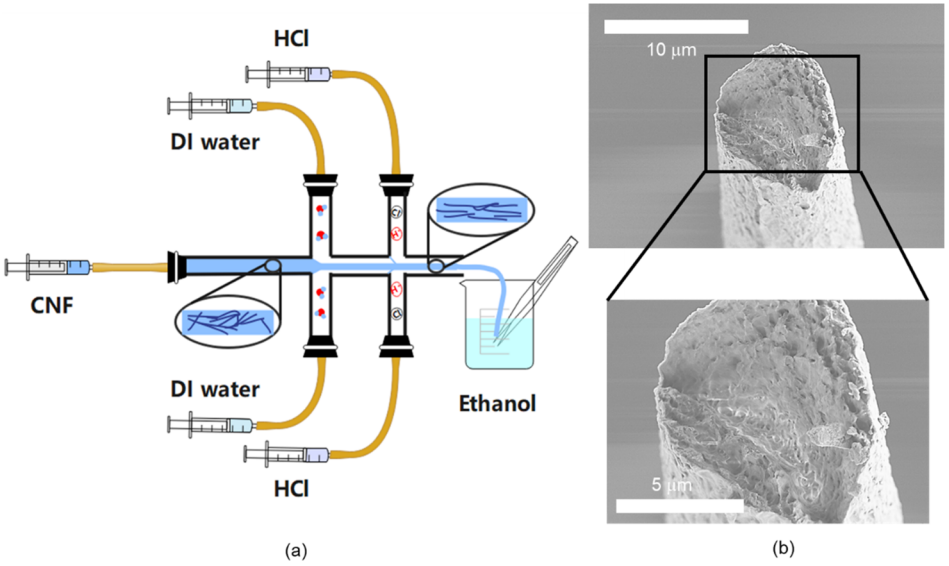

Figure 1. Preparation and characterization of CNF filaments with high thermal conductivity. (a) Schematic of the flow-focusing system[29] for fabricating CNF filaments. (b) Scanning electron microscopy images of a CNF filament cross-section. The scale bars are provided in each image.

other polymer chains have shown that their thermal conductivity can be considerably increased by increasing their alignment at the molecular level and crystallinity.[9−12] Shrestha et al. applied stretching and macro heating to polyethylene macrofibers to improve the molecular alignment along the fiber axis and found that the thermal conductivity of the resulting materials increased to 60 W/m-K at 300 K.[13] Xu et al. extruded a thin film made of polyethylene powder 110 times to disentangle and align the polymer molecules in amorphous regions and obtained a high thermal conductivity of 62 W/m-K.[14] Shen et al. reported the fabrication of high-quality, ultradrawn polyethylene with high thermal conductivity (∼104 W/m-K) and attributed their findings to the formation of restructured single-crystalline polymeric chains.[15] These studies have encouraged attempts to enhance the thermal conductivity of cellulose materials by aligning molecules or nanofibrils.

In this work, we fabricated high-thermal-conductivity cellulose nanofibril (CNF) filaments with enhanced alignment and crystallinity by hydrodynamically aligning and bonding individual constituent CNFs. We observed a record-high thermal conductivity of 14.5 W/m-K in a single cellulose filament. The thermal conductivity of our cellulose filaments largely exceeded that of cellulose thin films (∼1.5 W/m-K) and other pure cellulose-based materials.[16] We then investigated the structure of the filaments using Raman spectroscopy to understand the morphological factors leading to the observed enhancement in thermal conductivity. We found that filaments with high thermal conductivity had high crystallinity, resulting from the alignment and ion-induced gelation of CNFs during the flow-focusing process. During this process, shear and extensional flows aligned the CNFs and induced the ionic bonding of the CNFs.[17] Our findings demonstrate that modifying the surface activity of cellulose molecules could give rise to materials with enhanced crystallinity and, hence, thermal conductivity. The results collectively indicate that nanocellulose is a highly attractive material for thermal management applications.

The filaments with various diameters were fabricated by the flow-focusing system as shown in Figure 1. The overall thermal conductivity measurements of the cellulose filaments are shown in Figure 2. The diameters of the filaments range

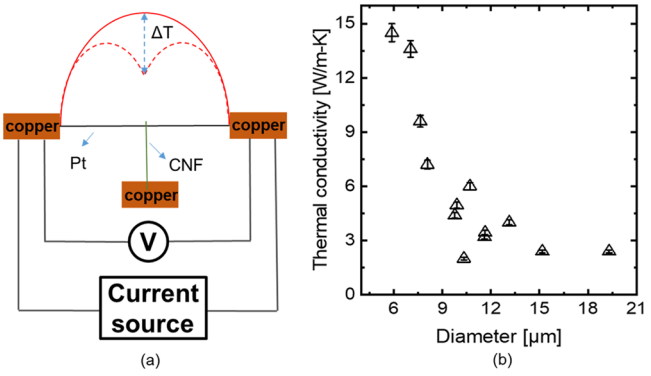

Figure 2. Thermal conductivity measurement of the CNF filaments. (a) Schematic of the self-built T-type steady-state measurement setup. The temperature distribution along the platinum wire is generated by Joule heating with/without a CNF filament attached to the platinum wire. (b) Measured thermal conductivity as a function of filament diameter. The error bars of thermal conductivity consider the uncertainties of the measured diameter, thermal conductance, and cross-sectional area.

from 6 to 20 μm, and their average thermal conductivity ranges from 2 to 14.5 W/m-K, which is higher than that previously reported for pure cellulose-based materials.[18] For instance, it is approximately five times those of cellulose nanopaper (∼2 W/m-K) and cellulose nanocrystals (∼3.5 W/m-K). Samples with smaller diameters tend to have higher thermal conductivities. Because theories suggest that the thermal conductivity of individual crystalline polymer chains can be increased by increasing the orientation and crystallinity of the crystallites,[10,11,14,15,19] the effects of crystallinity and orientation on the thermal conductivity of the filaments were investigated further.

In terms of the size of the crystal regions, Rbihi et al. found that improving the crystal size of cellulose could improve the thermal conductivity of cellulose aerogels.[20] During the flow-

https://doi.org/10.1021/acs.nanolett.2c02057
Nano Lett. 2022, 22, 8406−8412

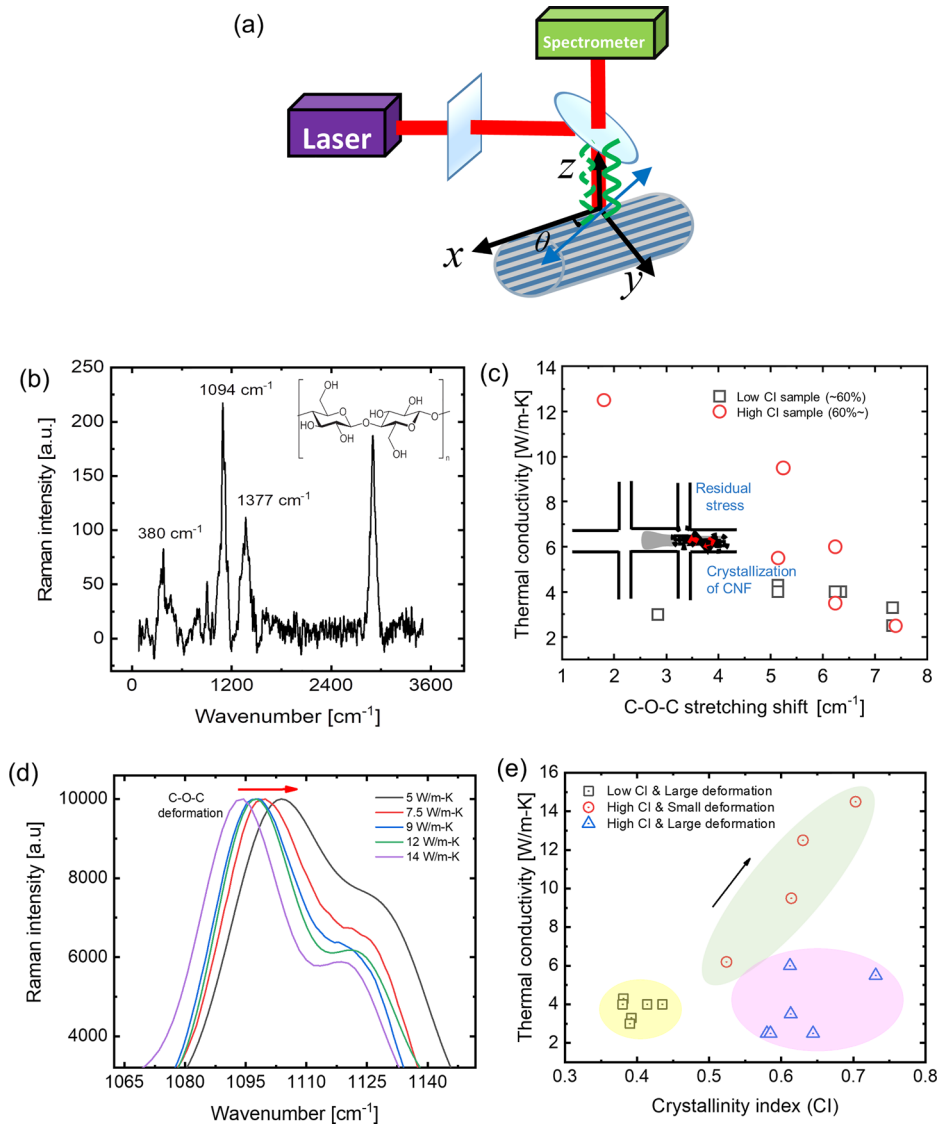

Figure 3. Structural characterization by Raman spectroscopy. (a) Schematic of the setup for Raman measurements. The beam was not polarized for both the incident and scattered light. (b) Typical Raman spectrum of CNF filaments highlighting the peaks at 380, 1096, and 1377 cm^{-1}. (c) Relations between the thermal conductivity and C−O−C stretching of high (>60%)- and low (<60%)-CI samples, where CI stands for crystallinity index. (d) Correlations between the Raman shift and thermal conductivity of the CNF filaments. (e) Dependence of thermal conductivity on CI of the CNF filaments. Data are grouped as follows: low CI and high C−O−C deformation (yellow), high CI and high C−O−C deformation (purple), and high CI and low C−O−C deformation (green).

focusing process, gelation occurs first at the surface region and then at the central region of the filament owing to the diffusive penetration of ions from the sheath flow. Daicho et al. found that inter-CNF hydrogen bonding contributes to an increase in crystallinity;[21] thus, we hypothesize that hydrogen bonding also enhances the crystallinity of the generated filaments. However, during the crystallization of cellulose, residual stresses are expected to form within the CNFs when the gelation crystals are unevenly distributed between two or more regions. The formation of residual stresses inside the filaments then alters their crystallinity.

Because the axial direction of CNF is parallel to that of the flow channel, the residual strain can be reflected by the Raman peak shift of the bonds (1096 cm^{-1}) along the main chain of the cellulose molecule due to the C−O−C bonding of two glucose molecules. Figure 3 shows the deformation of the C−O−C bond owing to the residual stress brought about by the uneven formation of hydrogen bonds between CNFs during the crystallization of CNF. It also shows the relationship between this deformation and the thermal conductivity of the filaments under different crystallinity index, CI, obtained from peak intensity ratios of Raman spectrum at 380 and 1096 cm^{-1}. CI has been found to correlate with the crystalline domain size[21] (see Supporting Information). Figure 3c reveals that a larger C−O−C deformation (larger residual stress) induces lower thermal conductivity and that filaments with lower C−O−C deformation tend to produce higher thermal conductivity in the high-CI samples (>60%). By contrast, filaments with lower CI (<60%) tend to have lower thermal conductivities (<4 W/m-K). Even for high-CI filaments, a relatively high C−O−C deformation also leads to reduced thermal conductivity. This is understandable since even when the crystalline domain is effectively large, if the crystal is disordered, that would scatter phonon and resist thermal

https://doi.org/10.1021/acs.nanolett.2c02057
Nano Lett. 2022, 22, 8406−8412

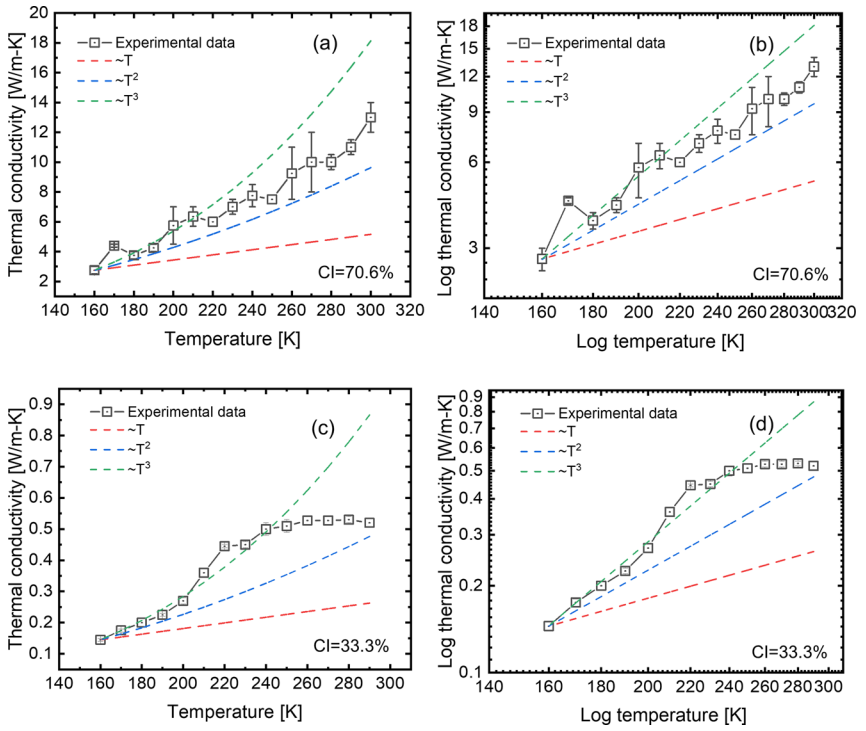

Figure 4. Temperature dependence of the thermal conductivity of (a,b) high (71%)- and (c,d) low (33%)-CI CNF filaments in the temperature range of 160−300 K.

transport. These findings agree with the hypothesis that residual stress generated during the gelation process is among the reasons behind the decrease in crystallinity, which, in turn, decreases the thermal conductivity of the filaments. Thus, the crystallinity of the cellulose filaments plays an important role in their thermal conductivity.

The crystallinity of the filaments along the radial direction was also characterized to understand the crystal formation process by hydrogen-bonding CNFs. Nonpolarized Raman measurements were performed along the radial direction by varying the focus on the test sample from the surface to the maximum probing depth, with a step depth of 0.7 μm (Figures S-7 and S-9, Supporting Information). The Raman spectra reveal that CI decreases along the radial direction (Figure S-7). The intensity of the normalized peak at 1096 cm^{-1} indicates that amount of −COONa is larger in the center of the filament, and smaller on the surface (Figure S-9). Since the charged negative carboxyl group should be bonded with either sodium ion or hydrogen ion, this suggests that the amount of − COOH is rich on the surface and becomes less toward the center. According to Daicho et al.,[21] filament crystallinity increases by protonation of the carboxylate groups. This finding verifies the hypothesis that the crystallization of the CNF filaments begins at their outer surface and continues toward their center. The gelation of cellulose is imposed by the infiltration of ions, thereby completing our explanation of the finding that smaller-diameter filaments tend to have higher thermal conductivity and greater crystallinity compared with larger-diameter samples. In addition, we performed micro-Fourier-transform infrared spectroscopy (Micro-FT-IR) to prove the variation of hydrogen bonds in filaments with different diameters (small, medium and large diameter). As shown in Figure S-10, the obtained absorption spectra in the region between 3000 and 3600 cm^{-1}, corresponding to the stretching vibration of hydrogen bonds, shows that wave-numbers of the peaks red-shift and the distribution of the peaks become narrower with decreasing diameter.[22] By strengthening the hydrogen bonds, H of hydroxyl group (−OH) is pulled toward acceptor and the distance between O (donor) and H of −OH is increased. As a result, the peak shifts to a lower wavenumber. In addition, hydrogen-bonded hydroxyl groups have some fixed bond distance, so the more hydrogen-bonded atoms, the narrower the peak distribution becomes. Therefore, the observed diameter dependence of the spectrum confirms that the number of hydrogen bonds increases with reducing diameter, thus enhancing thermal conductivity.

To improve our understanding of heat conduction through CNF filaments in the axial direction, we measured temperature dependence of the thermal conductivity of the filaments in the temperature range of 150−300 K, as shown in Figure 4. We measured two representative filaments: one with a high CI of 70.6% and the other with a low CI of 33.3%. Because the influence of structure on thermal conductivity is manifested by the temperature dependence of this property, comparative analysis was performed to assess the underlying mechanisms of nanostructure-mediated thermal phonon transport.

The heat in undoped semiconductors and insulators is predominantly carried by phonon, the quantized lattice vibration. The phonon gas model is often adopted to describe phonon transport in crystals and has helped researchers understand heat conduction mechanisms from a microscopic viewpoint, which is particularly useful for nanostructures. The kinetics of a phonon gas can be solved by the Boltzmann transport equation. When linearized by relaxation time approximation, thermal conductivity can be written as

$$\kappa(T) = \frac{1}{3}\sum_i \int C_i(\omega, T) v_i l_i(\omega, T) \mathrm{d}\omega \quad (1)$$

https://doi.org/10.1021/acs.nanolett.2c02057
Nano Lett. 2022, 22, 8406−8412

where $C_i(\omega)$ is the heat capacity, ω is the frequency, T is the temperature, v_i is the group velocity, and $l_i(\omega)$ is the mean free path of phonon. At temperatures lower than the Debye temperature, $C_i(\omega)$ is proportional to T^3 for 3D systems and T^2 for 2D systems.[23] In the present study, strong interactions among the constituent CNFs of our filaments led to phonon transport not only in the axial direction but also in the radial direction. Therefore, we expect the dimension of phonon transport to lie between the 2D and 3D systems. At temperatures higher than the Debye temperature, the quantum effects become negligible and $C_i(\omega)$ becomes constant. The group velocity can be obtained by analyzing harmonic phonon dispersion relations and, thus, may generally be assumed to be independent of temperature.

The mean free path l_i, when larger than the grain size L_0, is limited by boundary scattering and can be written as

$$\frac{1}{l_i} = \frac{1}{l_0} + \frac{1}{L_0} \tag{2}$$

where l_0 is the intrinsic mean free path determined by phonon−phonon scattering. l_0 is typically proportional to T^{-1} for crystalline materials, and the temperature dependence becomes weaker for disordered materials. Therefore, for crystalline materials with grain boundaries, phonon−phonon scattering dominates and l_i scales with T^{-1} at high temperatures whereas boundary scattering dominates and the temperature dependence weakens at low temperatures. The presence of partial disorder further weakens the overall temperature dependence.

The above discussion suggests that the thermal conductivity of CNF filaments at low temperatures would rapidly increase with increasing temperature and exhibit a peak before it decreases or becomes nearly constant at higher temperatures. The peaking or flattening temperature depends on the effective Debye temperature and mean free path. The influence of mean free path is rather straightforward that lower crystallinity decreases the mean free path tending the peak to shift toward lower temperature. On the other hand, the influence of Debye temperature is nontrivial. In the case of a system consisting of bundles of molecular chains, such as nanocellulose filaments, the larger the number and strength of interfibril bonds (i.e., crystallinity), the larger the effective Debye temperature,[24] and thus, the higher the peaking and flattening temperatures.

The temperature dependence of the thermal conductivity of other polymer chains has been discussed in the literature. Shrestha et al.[13] observed that the thermal conductivity of polyethylene crystalline nanofibers decreases as a function of T^{-1} at temperatures above 130 K. Antlauf et al.[23] found that the thermal conductivity of macro-sized cellulose fibers increases from 100 to 300 K. This difference may be explained by the dominance of amorphous regions in the cellulose fibers and the high Debye temperature of these fibers. Moreover, the temperature dependence of thermal conductivity of celllulose fibers may show a decreasing trend at relatively high temperature ranges. Another study by Dong et al.[25] showed that the thermal conductivity of cellulose nanocrystals with an effective structure size of 21.8 nm decreases when the temperature reaches 350 K.

The experimental results in Figure 4 show that the thermal conductivity of filaments with higher CI increases steeply with the temperature up to 300 K. The thermal conductivity of filaments with lower CI also increases with a similar slope until 240 K, but then saturates to a constant value until 300 K. Based on the above discussion of the temperature dependence of thermal conductivity, the steep increase in thermal conductivity is due to the contribution of $C_i(\omega)$ in eq 1, and the flattening observed for filaments with low CI is due to fewer and weaker interfibril bonds, which reduce the effective Debye temperature. The peaking or flattening temperatures in both cases are higher than that of polyethylene crystalline nanofibers owing to the high Debye temperature of bulk cellulose materials.[24] For instance, the Debye temperature of cotton and wood cellulose is reported to be approximately 920 K, which is significantly higher than the Debye temperature of polyethylene (400 K).[24] Debye temperature increases with enhanced interatomic force constant and lattice orderliness for materials with the same composition. Hydrogen-bond-induced crystallization discussed in this work increases both the effective force constant and lattice orderliness and thus we suggested the relation to the Debye temperature. It should be noted that the residual strain or corresponding local disorder also reduces the orderliness, and thus, can alter the Debye temperature. However, its influence on the interatomic force constant is not simple, as it is known that bond stretching can influence differently depending on the phonon modes even in one material.

We also investigated the power-law exponent of the temperature dependence of thermal conductivity by taking the logarithm of thermal conductivity and temperature, as shown in Figure 4. Both high-and low-crystallinity filaments revealed exponents between 2 and 3. In this regime, the heat capacity is expected to dominate the trend of the temperature dependence, as discussed above. Here, as can be understood from eq 1, it is not the overall heat capacity that contributes to thermal conductivity, but it is the heat capacity of the modes, which can be directional to some extent in such aligned systems. In this sense, the obtained exponents indicate that the effective dimension of thermal transport of the CNF filaments is between 2D and 3D. Note that the temperature dependence could also be influence by disorder scattering. However, when comparing the temperature dependences at low temperatures of high and low crystallinity filaments, the dependence of the former is not larger than the latter. This and the fact that the dimension of their structures is similar suggest the leading contribution of $C_i(\omega)$ in determining the temperature dependence of thermal conductivity in the low temperature region.

In summary, we prepared a series of cellulose filaments using a hydrodynamic flow-focusing channel system. The approach allows for the simultaneous control of the crystallinity and orientation of CNFs in the bulk filaments, which are thus endowed with high thermal conductivity. We obtained a maximum thermal conductivity of 14.5 W/m-K, which is 4−5 times higher than that of other similar cellulose materials, including filaments, nanofibers, and thin films. Considering their high thermal conductivity, considerable renewability, low weight, excellent mechanical properties, and flexibility, the cellulose filaments have potential applications as novel thermal management materials.

EXPERIMENTAL SECTION

Preparing Cellulose Filaments and Morphology of Filaments. A TEMPO−CNF dispersion was mechanically treated using a homogenizer to achieve CNFs with a uniform length, ultracentrifugated to remove impurities, and ultrasonically oscillated to separate stable CNFs. The filaments were

https://doi.org/10.1021/acs.nanolett.2c02057
Nano Lett. 2022, 22, 8406−8412

prepared via hydrodynamic assembly in the flow focusing channel system to induce the alignment of CNFs (Figure 1).[26] The shear force generated by the injected distilled water in sheath flow 1 makes the CNFs orient in the flow direction. Hydrochloric acid was injected in sheath flow 2 to improve the alignment of CNFs, which were then gelated into a gel thread by the diffusion of hydrogen ions. The gel thread was ejected into an ethanol bath, where solvent exchange occurs to accelerate evaporation. Finally, the gel threads were removed from the ethanol bath and dried. More details of the fabrication can be found in Supporting Information.

Thermal Conductivity Measurement. We utilized the T-type thermal conductivity measurement setup shown in Figure 2 to investigate the thermal properties of our cellulose filaments under vacuum conditions ($<10^{-4}$ Pa). When a test sample is attached to the platinum wire, heat is conducted through the test sample via the middle junction point, and the temperature varies along the platinum wire. From this variation, the thermal conductivity of the cellulose filament at the T-junction can be extracted using a physical model. More details of the measurement can be found in Supporting Information.

Structure Investigation. The crystallinity index (CI) extracted from Raman spectroscopy was used to measure the mass percentage of crystalline regions in the whole cellulose material.[27] We adopt a CI calculated from intensity ratio of Raman peaks at 380 and 1096 cm^{-1} as follows

$$\text{Crystallinity index} = \frac{(I_{380}/I_{1096}) - 0.0286}{0.0065} \quad (3)$$

This CI has been found to correlated with the crystal domain size for various biomaterials.[28] Raman spectroscopy was also used to identified the orientation of CNFs. We adopted linear polarization for both the incident (parallel to the axial direction of the filament) and scattered light and normalized the peak intensity at 1377 cm^{-1} with that at 1096 cm^{-1} to identify the orientation of the CNFs. Note while orientation is a necessary condition to achieve high thermal conductivity, it is not a sufficient condition. This can be understood from the Figure S-8a,b, where orientation is not correlated with thermal conductivity (i.e., crystallinity) nor residual strain.

■ ASSOCIATED CONTENT

Supporting Information

The Supporting Information is available free of charge at https://pubs.acs.org/doi/10.1021/acs.nanolett.2c02057.

Additional experimental information (PDF)

■ AUTHOR INFORMATION

Corresponding Author

Junichiro Shiomi − *Department of Mechanical Engineering, Graduate School of Engineering, The University of Tokyo, Bunkyo-ku, Tokyo 113-8656, Japan; Institute of Engineering Innovation, Graduate School of Engineering, The University of Tokyo, Bunkyo-ku, Tokyo 113-0032, Japan;* orcid.org/0000-0002-3552-4555; Email: shiomi@photon.t.u-tokyo.ac.jp

Authors

Guantong Wang − *Department of Mechanical Engineering, Graduate School of Engineering, The University of Tokyo, Bunkyo-ku, Tokyo 113-8656, Japan*

Masaki Kudo − *Department of Mechanical Engineering, Graduate School of Engineering, The University of Tokyo, Bunkyo-ku, Tokyo 113-8656, Japan; Mechanical Systems Engineering Program, Tokyo Metropolitan College of Industrial Technology, Shinagawa-ku, Tokyo 140-0011, Japan;* orcid.org/0000-0002-1744-9993

Kazuho Daicho − *Department of Biomaterials Science, Graduate School of Agricultural and Life Sciences, The University of Tokyo, Tokyo 113-8657, Japan;* orcid.org/0000-0003-4203-2257

Sivasankaran Harish − *Department of Mechanical Engineering, Graduate School of Engineering, The University of Tokyo, Bunkyo-ku, Tokyo 113-8656, Japan*

Bin Xu − *Department of Mechanical Engineering, Graduate School of Engineering, The University of Tokyo, Bunkyo-ku, Tokyo 113-8656, Japan*

Cheng Shao − *Department of Mechanical Engineering, Graduate School of Engineering, The University of Tokyo, Bunkyo-ku, Tokyo 113-8656, Japan*

Yaerim Lee − *Department of Mechanical Engineering, Graduate School of Engineering, The University of Tokyo, Bunkyo-ku, Tokyo 113-8656, Japan*

Yuxuan Liao − *Department of Mechanical Engineering, Graduate School of Engineering, The University of Tokyo, Bunkyo-ku, Tokyo 113-8656, Japan*

Naoto Matsushima − *Department of Mechanical Engineering, Graduate School of Engineering, The University of Tokyo, Bunkyo-ku, Tokyo 113-8656, Japan*

Takashi Kodama − *Department of Mechanical Engineering, Graduate School of Engineering, The University of Tokyo, Bunkyo-ku, Tokyo 113-8656, Japan;* orcid.org/0000-0002-8753-5766

Fredrik Lundell − *Linné FLOW Centre, KTH Mechanics, KTH Royal Institute of Technology, Stockholm SE−100 44, Sweden;* orcid.org/0000-0002-2504-3969

L. Daniel Söderberg − *Linné FLOW Centre, KTH Mechanics, KTH Royal Institute of Technology, Stockholm SE−100 44, Sweden;* orcid.org/0000-0003-3737-0091

Tsuguyuki Saito − *Department of Biomaterials Science, Graduate School of Agricultural and Life Sciences, The University of Tokyo, Tokyo 113-8657, Japan;* orcid.org/0000-0003-1073-6663

Complete contact information is available at: https://pubs.acs.org/10.1021/acs.nanolett.2c02057

Notes

The authors declare no competing financial interest.

■ ACKNOWLEDGMENTS

This work was partially supported by JSPS KAKENHI (Grants 19K21928 and 22H04950) and JST CREST (JPMJCR21O2).

■ REFERENCES

(1) George, J.; Sabapathi, S. N. Cellulose Nanocrystals: Synthesis, Functional Properties, and Applications. *Nanotechnol. Sci. Appl.* **2015**, *8*, 45−54.

(2) Waliszewska, B.; Mleczek, M.; Zborowska, M.; Goliński, P.; Rutkowski, P.; Szentner, K. Changes in the Chemical Composition

and the Structure of Cellulose and Lignin in Elm Wood Exposed to Various Forms of Arsenic. *Cellulose* **2019**, *26* (10), 6303−6315.
(3) Isogai, A. Review Development of Completely Dispersed Cellulose Nano Fi Bers. *Proc. Jpn. Acad., Ser. B 94* **2018**, *94* (4), 161−179.
(4) Sakuma, W.; Yamasaki, S.; Fujisawa, S.; Kodama, T.; Shiomi, J.; Kanamori, K.; Saito, T. Mechanically Strong, Scalable, Mesoporous Xerogels of Nanocellulose Featuring Light Permeability, Thermal Insulation, and Flame Self-Extinction. *ACS Nano* **2021**, *15* (1), 1436−1444.
(5) Illera, D.; Mesa, J.; Gomez, H.; Maury, H. Cellulose Aerogels for Thermal Insulation in Buildings: Trends and Challenges. *Coatings* **2018**, *8* (10), 345.
(6) Sakai, K.; Kobayashi, Y.; Saito, T.; Isogai, A. Partitioned Airs at Microscale and Nanoscale: Thermal Diffusivity in Ultrahigh Porosity Solids of Nanocellulose. *Sci. Rep.* **2016**, *6* (1), 1−7.
(7) Apostolopoulou-Kalkavoura, V.; Munier, P.; Bergström, L. Thermally Insulating Nanocellulose-Based Materials. *Adv. Mater.* **2021**, *33* (28), 2001839.
(8) Uetani, K.; Hatori, K. Thermal Conductivity Analysis and Applications of Nanocellulose Materials. *Sci. Technol. Adv. Mater.* **2017**, *18* (1), 877−892.
(9) Shen, S.; Henry, A.; Tong, J.; Zheng, R.; Chen, G. Polyethylene Nanofibres with Very High Thermal Conductivities. *Nat. Nanotechnol.* **2010**, *5* (4), 251−255.
(10) Wang, X.; Ho, V.; Segalman, R. A.; Cahill, D. G. Thermal Conductivity of High-Modulus Polymer Fibers. *Macromolecules* **2013**, *46* (12), 4937−4943.
(11) Zhu, B.; Liu, J.; Wang, T.; Han, M.; Valloppilly, S.; Xu, S.; Wang, X. Novel Polyethylene Fibers of Very High Thermal Conductivity Enabled by Amorphous Restructuring. *ACS Omega* **2017**, *2* (7), 3931−3944.
(12) Singh, V.; Bougher, T. L.; Weathers, A.; Cai, Y.; Bi, K.; Pettes, M. T.; McMenamin, S. A.; Lv, W.; Resler, D. P.; Gattuso, T. R.; Altman, D. H.; Sandhage, K. H.; Shi, L.; Henry, A.; Cola, B. A. High Thermal Conductivity of Chain-Oriented Amorphous Polythiophene. *Nat. Nanotechnol.* **2014**, *9* (5), 384−390.
(13) Shrestha, R.; Li, P.; Chatterjee, B.; Zheng, T.; Wu, X.; Liu, Z.; Luo, T.; Choi, S.; Hippalgaonkar, K.; De Boer, M. P.; Shen, S. Crystalline Polymer Nanofibers with Ultra-High Strength and Thermal Conductivity. *Nat. Commun.* **2018**, *9* (1), 1−9.
(14) Xu, Y.; Kraemer, D.; Song, B.; Jiang, Z.; Zhou, J.; Loomis, J.; Wang, J.; Li, M.; Ghasemi, H.; Huang, X.; Li, X.; Chen, G. Nanostructured Polymer Films with Metal-like Thermal Conductivity. *Nat. Commun.* **2019**, *10* (1), 1771.
(15) Shen, S.; Henry, A.; Tong, J.; Zheng, R.; Chen, G. Polyethylene Nanofibres with Very High Thermal Conductivities. *Nat. Nanotechnol.* **2010**, *5* (4), 251−255.
(16) Yang, W.; Zhao, Z.; Wu, K.; Huang, R.; Liu, T.; Jiang, H.; Chen, F.; Fu, Q. Ultrathin Flexible Reduced Graphene Oxide/Cellulose Nanofiber Composite Films with Strongly Anisotropic Thermal Conductivity and Efficient. *Journnl of Mater Chem C* **2017**, *5*, 3748−3756.
(17) Gowda, V. K.; Rosén, T.; Roth, S. V.; Söderberg, L. D.; Lundell, F. Nanofibril Alignment during Assembly Revealed by an X-Ray Scattering-Based Digital Twin. *ACS Nano* **2022**, *16* (2), 2120−2132.
(18) Yang, W.; Zhao, Z.; Wu, K.; Huang, R.; Liu, T.; Jiang, H.; Chen, F.; Fu, Q. Ultrathin Flexible Reduced Graphene Oxide/Cellulose Nanofiber Composite Films with Strongly Anisotropic Thermal Conductivity and Efficient Electromagnetic Interference Shielding. *J. Mater. Chem. C* **2017**, *5* (15), 3748−3756.
(19) Resler, D. P.; Singh, V.; Cai, Y.; Bi, K.; Bougher, T. L.; Cola, B. A.; Sandhage, K. H.; Shi, L.; Weathers, A.; Altman, D. H.; McMenamin, S. A.; Lv, W.; Henry, A.; Pettes, M. T.; Gattuso, T. R. High Thermal Conductivity of Chain-Oriented Amorphous Polythiophene. *Nat. Nanotechnol.* **2014**, *9* (5), 384−390.
(20) Rbihi, S.; Laallam, L.; Sajieddine, M.; Jouaiti, A. Characterization and Thermal Conductivity of Cellulose Based Composite Xerogels. *Heliyon* **2019**, *5* (5), No. e01704.
(21) Daicho, K.; Kobayashi, K.; Fujisawa, S.; Saito, T. Recovery of the Irreversible Crystallinity of Nanocellulose by Crystallite Fusion: A Strategy for Achieving Efficient Energy Transfers in Sustainable Biopolymer Skeletons**. *Angew. Chemie - Int. Ed.* **2021**, *60* (46), 24630−24636.
(22) Makarem, M.; Lee, C. M.; Kafle, K.; Huang, S.; Chae, I.; Yang, H.; Kubicki, J. D.; Kim, S. H.*Probing Cellulose Structures with Vibrational Spectroscopy*; Springer Netherlands, 2019; Vol. *26*.
(23) Antlauf, M.; Boulanger, N.; Berglund, L.; Oksman, K.; Andersson, O. Thermal Conductivity of Cellulose Fibers in Different Size Scales and Densities. *Biomacromolecules* **2021**, *22* (9), 3800−3809.
(24) Thybring, E. E. Explaining the Heat Capacity of Wood Constituents by Molecular Vibrations. *J. Mater. Sci.* **2014**, *49* (3), 1317−1327.
(25) Dong, R.-Y.; Dong, Y.; Li, Q.; Wan, C. Ballistic-Diffusive Phonon Transport in Cellulose Nanocrystals by ReaxFF Molecular Dynamics Simulations. *Int. J. Heat Mass Transfer* **2020**, *148*, 119155.
(26) Håkansson, K. M. O. Online Determination of Anisotropy during Cellulose Nanofibril Assembly in a Flow Focusing Device. *RSC Adv.* **2015**, *5* (24), 18601−18608.
(27) Ralph, S. A. *Cellulose I Crystallinity Determination Using FT - Raman Spectroscopy : Univariate and Multivariate Methods* **2010**, 721−733.
(28) Agarwal, U. P.; Reiner, R. S.; Ralph, S. A. Cellulose I Crystallinity Determination Using FT-Raman Spectroscopy: Univariate and Multivariate Methods. *Cellulose* **2010**, *17* (4), 721−733.
(29) Håkansson, K. M. O.; Fall, A. B.; Lundell, F.; Yu, S.; Krywka, C.; Roth, S. V.; Santoro, G.; Kvick, M.; Prahl Wittberg, L.; Wågberg, L.; Söderberg, L. D. Hydrodynamic Alignment and Assembly of Nanofibrils Resulting in Strong Cellulose Filaments. *Nat. Commun.* **2014**, *5* (1), 1−10.

NOTE ADDED AFTER ASAP PUBLICATION

Due to a production error, this paper was published ASAP on October 25, 2022, with errors in the TOC/abstract graphic and Figures 3 and 4. The corrected version was reposted on October 26, 2022.

https://doi.org/10.1021/acs.nanolett.2c02057
Nano Lett. 2022, 22, 8406−8412